Ca^{2+} marks: Miniature calcium signals in single mitochondria driven by ryanodine receptors

Pál Pacher*, Andrew P. Thomas†, and György Hajnóczky*‡

*Department of Pathology, Anatomy, and Cell Biology, Thomas Jefferson University, Philadelphia, PA 19107; and †Department of Pharmacology and Physiology, University of Medicine and Dentistry of New Jersey–New Jersey Medical School, Newark, NJ 07103

Edited by Clara Franzini-Armstrong, University of Pennsylvania School of Medicine, Philadelphia, PA, and approved December 6, 2001 (received for review August 10, 2001)

Propagation of cytosolic $[Ca^{2+}]$ ($[Ca^{2+}]_c$) signals to the mitochondria is believed to be supported by a local communication between Ca^{2+} release channels and adjacent mitochondrial Ca^{2+} uptake sites, but the signaling machinery has not been explored at the level of elementary Ca^{2+} release events. Here, we demonstrate that $[Ca^{2+}]_c$ sparks mediated by ryanodine receptors are competent to elicit miniature mitochondrial matrix $[Ca^{2+}]$ signals that we call ''Ca^{2+} marks.'' Ca^{2+} marks are restricted to single mitochondria and typically last less than 500 ms. The decay of Ca^{2+} marks relies on extrusion of Ca^{2+} from the mitochondria through the Ca^{2+} exchanger, whereas $[Ca^{2+}]_c$ sparks decline primarily by diffusion. Mitochondria also appear to have a direct effect on the properties of $[Ca^{2+}]_c$ sparks, because inhibition of mitochondrial Ca^{2+} uptake results in an increase in the frequency and duration of $[Ca^{2+}]_c$ sparks. Thus, a short-lasting opening of a cluster of Ca^{2+} release channels can yield activation of mitochondrial Ca^{2+} uptake, and the competency of mitochondrial Ca^{2+} handling may be an important determinant of cardiac excitability through local feedback control of elementary $[Ca^{2+}]_c$ signals.

calcium signaling | sparks | mitochondrial calcium | cardiac excitability

Recent improvements in microscopic imaging have facilitated visualization of the activity of small groups of Ca^{2+} release channels as elementary cytosolic $[Ca^{2+}]$ ($[Ca^{2+}]_c$) signals, sparks, and puffs (1–3). Calcium sparks and puffs may establish local regulation of Ca^{2+} targets in discrete subcellular domains, and, via coordinated recruitment, the elementary events also may give rise to global $[Ca^{2+}]_c$ signals. Local $[Ca^{2+}]_c$ control is thought to be pivotal for many Ca^{2+}-dependent processes (for review, see refs. 4 and 5), but downstream effects of the individual elementary events have been difficult to resolve. Given the local communication between Ca^{2+} release channels and adjacent mitochondrial Ca^{2+} uptake sites, mitochondria have been suggested to respond to spatially confined Ca^{2+} release (6–13). Furthermore, if mitochondrial Ca^{2+} uptake is activated in the effective domain of $[Ca^{2+}]_c$ sparks and puffs, mitochondria could actively contribute to the organization of elementary calcium signaling in the cytosol. However, propagation of $[Ca^{2+}]_c$ signals to the mitochondria has not been explored at the level of individual elementary Ca^{2+} release events.

Mitochondrial calcium signaling is important in the control of fundamental cellular functions including energy metabolism and apoptotic cell death (8, 14–17). Mitochondrial calcium signals often are established by Ca^{2+} release from sarco-endoplasmic reticulum Ca^{2+} stores as a result of the strategic localization of the low-affinity mitochondrial Ca^{2+} uptake sites close to Ca^{2+} release channels. This machinery has been shown to be effective in delivering Ca^{2+} to the mitochondria during $[Ca^{2+}]_c$ spikes (6–8, 10, 11, 18). Furthermore, Duchen *et al.* (19) monitored changes in mitochondrial membrane potential and demonstrated localized mitochondrial depolarizations in myocytes. Based on the association of depolarizations with contraction and on the effect of Ca^{2+} transport inhibitors, they concluded that the depolarizations were due to mitochondrial Ca^{2+} uptake. However, no measurement of localized cytosolic or mitochondrial matrix ($[Ca^{2+}]_m$) signals was shown in the study of Duchen *et al.* (19). Mitochondrial Ca^{2+} uptake may be associated with membrane depolarization, but there is no expectation of a relationship between membrane potential and the subsequent duration and decay of mitochondrial Ca^{2+}, which are the key parameters in the regulation of mitochondrial function. Moreover, mitochondrial Ca^{2+} uptake can be associated with an increase in membrane potential because of activation of metabolism (8, 20). Thus, it is of critical importance to measure mitochondrial Ca^{2+} directly and to address the question of whether brief opening of a few release channels during elementary Ca^{2+} release events, such as ryanodine receptor (RyR)-mediated Ca^{2+} sparks and IP_3 receptor-mediated Ca^{2+} puffs, is sufficient to trigger $[Ca^{2+}]_m$ increases. The extent to which $[Ca^{2+}]_c$ sparks and puffs propagate to the mitochondria is a critical parameter for understanding the control of mitochondrial Ca^{2+} targets and the local feedback exerted by mitochondrial Ca^{2+} uptake on $[Ca^{2+}]_c$. Using confocal microscopy and compartmentalized rhod2 to image $[Ca^{2+}]$ at the level of individual mitochondria for the first time, we were able to record the elementary units of the $[Ca^{2+}]_m$ signal and to study how the miniature $[Ca^{2+}]_m$ rise is integrated into intracellular Ca^{2+} regulation.

Experimental Procedures

Cells and Solutions. H9c2 cardiac cells were cultured, plated for imaging, and allowed to differentiate to myotubes as described previously (21, 22). Before use, the cells were preincubated for 30 min in extracellular medium composed of 121 mM NaCl, 5 mM $NaHCO_3$, 10 mM Na·Hepes, 4.7 mM KCl, 1.2 mM KH_2PO_4, 1.2 mM $MgSO_4$, 2 mM $CaCl_2$, 10 mM glucose, and 2% BSA (pH 7.4) at 37°C. Loading with the dyes was carried out in the same buffer. For measurements of $[Ca^{2+}]_m$ in permeabilized myotubes, the cells were loaded with 4 μM rhod2/AM in the presence of 0.003% (wt/vol) pluronic acid at 37°C for 50 min. Dye-loaded cells were washed with Ca^{2+}-free extracellular buffer composed of 120 mM NaCl, 20 mM Na·Hepes, 5 mM KCl, 1 mM KH_2PO_4, and 100 μM EGTA/Tris at pH 7.4 and then permeabilized with 15–20 μg/ml digitonin for 4 min in intracellular medium (ICM) composed of 120 mM KCl, 10 mM NaCl, 1 mM KH_2PO_4, 20 mM Tris·Hepes, and 2 mM MgATP at pH 7.2, supplemented with 1 μg/ml each of antipain, leupeptin, and pepstatin (21, 22). For fluorescence imaging of $[Ca^{2+}]_c$, labeling of cells with fura-C_{18} (1 μM) was carried out during permeabilization. All of the measurements were performed in the presence of 2 mM succinate, 2 mM MgATP, and an ATP-regenerating system composed of 5 mM phosphocreatine and 5

This paper was submitted directly (Track II) to the PNAS office.

Abbreviations: $[Ca^{2+}]_c$, cytosolic $[Ca^{2+}]$; RyR, ryanodine receptor.

‡To whom reprint requests should be addressed at: Department of Pathology, Anatomy and Cell Biology, 1020 Locust Street, Suite 253 JAH, Thomas Jefferson University, Philadelphia, PA 19107. E-mail: Gyorgy.Hajnoczky@mail.tju.edu.

The publication costs of this article were defrayed in part by page charge payment. This article must therefore be hereby marked "*advertisement*" in accordance with 18 U.S.C. §1734 solely to indicate this fact.

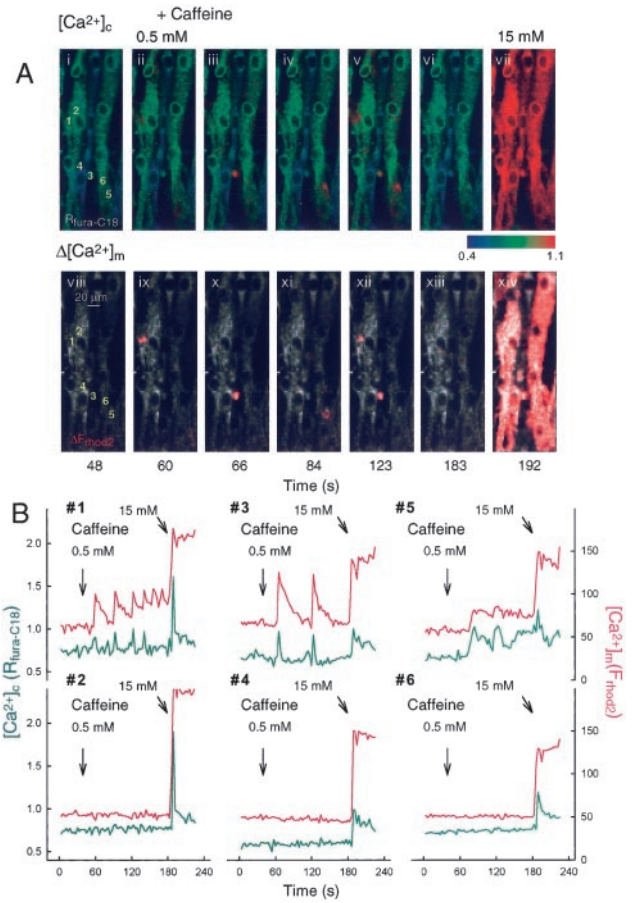

Fig. 1. Spatially restricted $[Ca^{2+}]_c$ and $[Ca^{2+}]_m$ spikes evoked by submaximal activation of the RyR. Fluorescence imaging of $[Ca^{2+}]_c$ and $[Ca^{2+}]_m$ responses evoked by caffeine in rhod2-loaded permeabilized myotubes was performed. (*A*) The pseudocolor ratio images (340 nm/380 nm; blue, low $[Ca^{2+}]$; red, high $[Ca^{2+}]$) in *Upper* show the changes in fura-C18 fluorescence ($[Ca^{2+}]_c$) after the addition of 0.5 mM (ii–vi) and 15 mM (vii) caffeine. The gray images in *Lower* show the rhod2 fluorescence ($[Ca^{2+}]_m$), and the red overlays show the fluorescence changes from increased $[Ca^{2+}]_m$ at each time point, measured simultaneously with $[Ca^{2+}]_c$. (*B*) Time courses of $[Ca^{2+}]_c$ and $[Ca^{2+}]_m$ changes for the numbered regions. Regions were selected in the areas displaying local $[Ca^{2+}]_c$ spiking in response to 0.5 mM caffeine (1, 3, 5) and in adjacent regions that exhibited a response only during stimulation with maximal caffeine (2, 4, 6). A $[Ca^{2+}]_m$ rise was coupled to every localized $[Ca^{2+}]_c$ spike in the selected regions (see graphs).

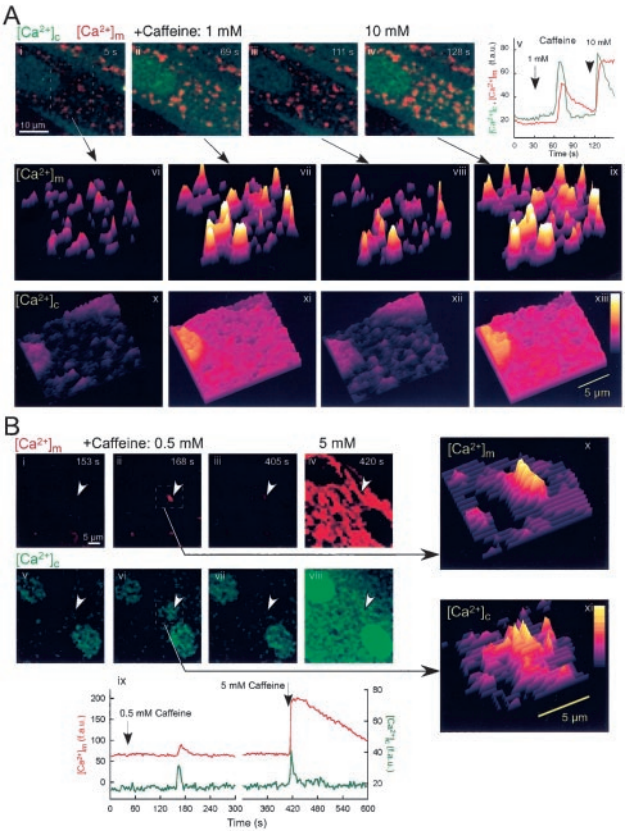

Fig. 2. $[Ca^{2+}]_m$ increases exhibited by individual mitochondria during RyR-mediated Ca^{2+} release. (*A*) Confocal imaging of $[Ca^{2+}]_m$ and $[Ca^{2+}]_c$ responses evoked by sequential addition of 1 mM and 10 mM caffeine in a rhod2-loaded permeabilized myotube. $[Ca^{2+}]_c$ was measured with fluo3 added to the intracellular buffer. Spatial organization of $[Ca^{2+}]_m$ and $[Ca^{2+}]_c$ changes in the region marked by the box in image i is presented as a series of three-dimensional plots. Surface plots were obtained by averaging three scans. Caffeine additions of 1 and 10 mM were made at 30 and 118 s, respectively (see graph in v). Global $[Ca^{2+}]_c$ responses evoked by submaximal (xi) and maximal (xiii) caffeine resulted in heterogeneous $[Ca^{2+}]_m$ increases at the level of single mitochondria (vii, ix). Plots in vi, x, and viii, xii represent the basal state just before addition of 1 and 10 mM caffeine, respectively. (*B*) Confocal imaging of localized $[Ca^{2+}]_m$ and $[Ca^{2+}]_c$ responses. Red images (i–iv) show the $[Ca^{2+}]_m$ whereas the green images (v–viii) show the $[Ca^{2+}]_c$ in permeabilized myotubes stimulated with 0.5 and 5 mM caffeine added at 58 and 415 s, respectively. Time courses of $[Ca^{2+}]_m$ and $[Ca^{2+}]_c$ at the region of local $[Ca^{2+}]_m$ elevation (masked area: $\approx 1.6\ \mu m \times 4\ \mu m$) are plotted in red and green, respectively (ix). Spatial organization of the $[Ca^{2+}]_m$ and $[Ca^{2+}]_c$ rise during stimulation with 0.5 mM caffeine in the region marked by the box in image ii is presented as a three-dimensional plots (x, xi).

units/ml creatine kinase. Although differentiation of the myoblasts has been shown to cause down-regulation of IP_3 receptors (22), heparin (25 μg/ml) also was added to ICM to prevent activation of any remaining IP_3 receptors. $[Ca^{2+}]$ did not exceed 250–350 nM in the medium (11). After permeabilization, the cells were washed into fresh buffer without digitonin and incubated in the imaging chamber at 35°C.

Fluorescence and Confocal Imaging. Fluorescence imaging was carried out by using an Olympus IX70 inverted microscope [×40, UApo340, numerical aperture (n.a.) 1.35 oil-immersion objective) fitted with a cooled charge-coupled device camera (PXL; Photometrics) and a scanning monochromator (DeltaRAM; PTI, South Brunswick, NJ) under computer control, as described previously (11, 22). Simultaneous detection of fura-C18 (340- and 380-nm excitation) and rhod2 (545-nm excitation) fluorescence was achieved by using a multiwavelength beamsplitter/emission filter combination (Chroma Technology, Brattleboro, VT). Image triplets were obtained every 2.2 s.

For confocal imaging of $[Ca^{2+}]_m$, myotubes were loaded with rhod2/AM as described (21), and to monitor $[Ca^{2+}]_c$ signals, 10 μM fluo3 and 3–4 μM $CaCl_2$ were added after cell permeabilization in ICM ($[Ca^{2+}]$ was adjusted to $\approx$200–300 nM). Confocal imaging of $[Ca^{2+}]_c$ and $[Ca^{2+}]_m$ was carried out by using a Bio-Rad MRC1024/2P imaging system equipped with a Kr/Ar-ion laser source (488- and 568-nm excitation) fitted to an Olympus IX70 inverted microscope [×40, UApo340, n.a. 1.35 (Fig. 2*B*); ×60, PlanApo, n.a. 1.4 oil-immersion objectives (Figs. 2*A*, 3, and 4)]. Rhod2 was excited at 568 nm, and fluo3 was excited at 488 nm.

For confocal line scanning of $[Ca^{2+}]_c$ in intact myotubes, the cells were loaded with 5 μM fluo3/AM in the presence of 0.003% (wt/vol) pluronic acid and 100 μM sulfinpyrazone at room temperature for 25 min. After washing of the dye-loaded myotubes, imaging measurements were performed in extracellular medium containing 0.25% BSA at 35C°. Elementary $[Ca^{2+}]_c$ signals in

PHYSIOLOGY

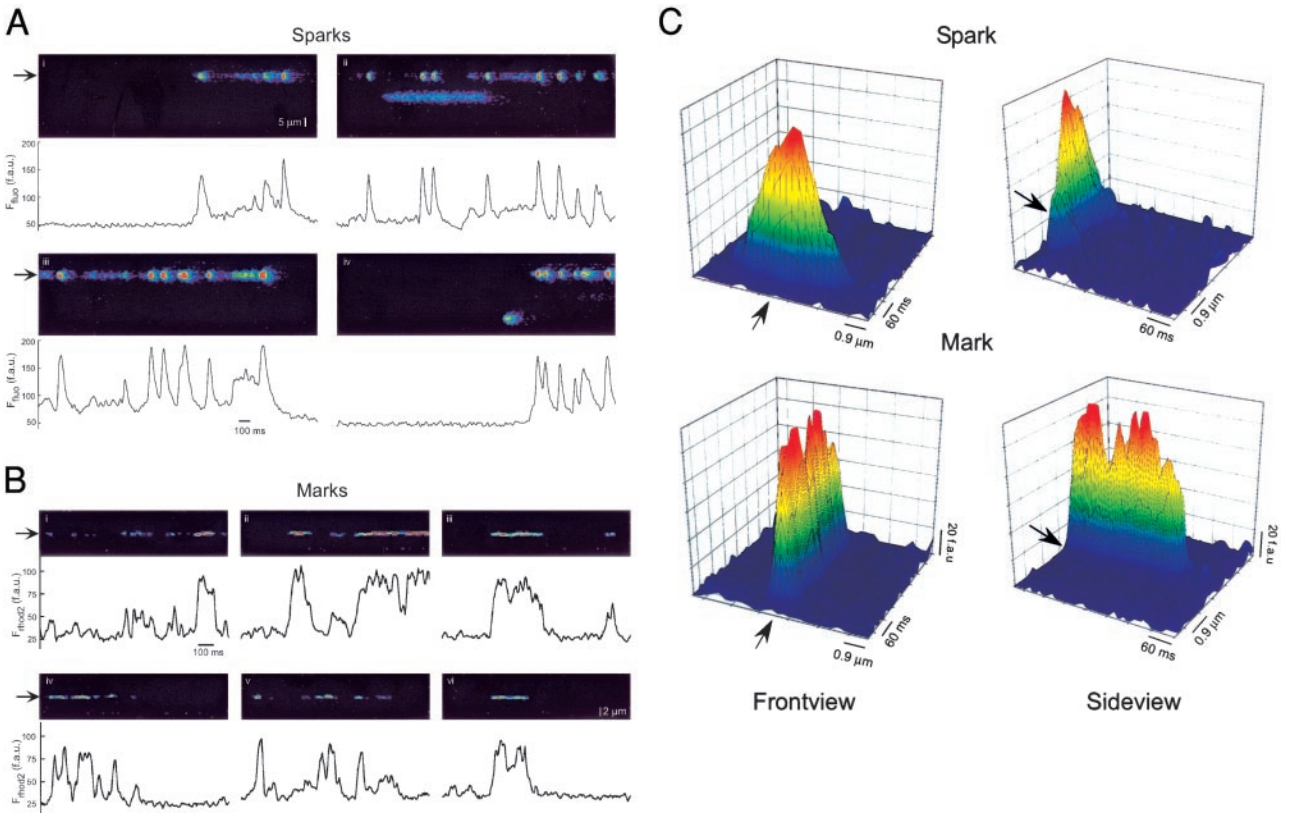

Fig. 3. $[Ca^{2+}]_c$ sparks and $[Ca^{2+}]_m$ marks in myotubes. (*A*) Representative linescan images of $[Ca^{2+}]_c$ sparks recorded in a fluo3-loaded myotube exposed to 0.25 mM caffeine. Successive lines are stacked horizontally; therefore, time is on the horizontal axis. Traces show fluorescence time courses for the site marked by the arrow. (*B*) Linescan images showing $[Ca^{2+}]_m$ marks in a rhod2-loaded, permeabilized myotube exposed to 0.25 mM caffeine. Traces show the temporal profile of fluorescence across a 1-μm region of the scan line, indicated by the solid arrow. The apparent plateau phase in some $[Ca^{2+}]_m$ increases was not due to saturation of rhod2, because the $[Ca^{2+}]_{rhod2}$ elevation was larger during global $[Ca^{2+}]_c$ waves (not shown). (*C*) Linescan images of a spark (second event in *A*, ii) and a mark (first event in *B*, iii) are presented as three-dimensional surfaces (front view, *Left*; side view, *Right*). The arrow indicates the direction of the time line.

permeabilized myotubes were recorded in the presence of 30 μM fluo3 and 8–9 μM $CaCl_2$ ($[Ca^{2+}]$ was adjusted to ≈200–300 nM). Linescan images were acquired by repeatedly scanning the laser beam along a single line [pixel size, 0.176 μm (Figs. 3*B* and 4) and 0.352 μm (Fig. 3*A*)] oriented with the long axis of a cell at 6-ms intervals. Linescan images were low-pass-filtered, averaging three pixels in each scan line and two pixels across scan lines (23) by using custom-designed software. Events that exhibit a rapid rise in fluorescence intensity, meeting the established criteria for $[Ca^{2+}]_c$ sparks (23), were analyzed for amplitude, width, and duration at half-maximum. The criteria applied to the fluo3 signal were also applied to the rhod2 signal to determine the amplitude, width, and duration at half-maximum of the $[Ca^{2+}]_m$ marks. In some cases, a second $[Ca^{2+}]_m$ rise appeared before 50% recovery of the first one (e.g., Fig. 3*B*, vi). To be considered a $[Ca^{2+}]_m$ mark, the second increase in F_{rhod2} had to be greater than the peak of the first one. Thus, we could fail to separate two events if the second one closely followed the first one and showed only a small rise in F_{rhod2}, and we could overestimate the duration of a small fraction of marks.

Data are presented as means ± SEM. The magnitude of the $[Ca^{2+}]_m$ increase during elementary $[Ca^{2+}]_m$ signals was calculated from rhod2 fluorescence by using the pseudoratio equation described previously for fluo3 (2), assuming that basal $[Ca^{2+}]_m$ in silent permeabilized cells was similar to $[Ca^{2+}]_c$ (200–300 nM) and the *in situ* K_d of rhod2 for Ca^{2+} was 1 μM. Similar to fluo3, the fluorescence of rhod2 in Ca^{2+}-free condition is minimal (<1% of maximum).

Results and Discussion

To investigate transmission of RyR-mediated localized $[Ca^{2+}]_c$ signals to the mitochondria, we first carried out simultaneous fluorescence imaging measurements of $[Ca^{2+}]_c$ and $[Ca^{2+}]_m$ in permeabilized cardiac myotubes by using fura-C18 anchored to cellular membranes and compartmentalized rhod2, respectively (21, 22). The permeabilized myotube preparation has the advantage that it allows direct access to the cytosol and mitochondria and the cytosolic component of rhod2 is eliminated. In response to suboptimal caffeine (0.5 mM), the myotubes displayed $[Ca^{2+}]_c$ spiking that was confined to small regions of the cells, whereas subsequent application of maximal caffeine yielded elevations in $[Ca^{2+}]_c$ throughout the cells (Fig. 1). During the localized $[Ca^{2+}]_c$ spikes, elevations of $[Ca^{2+}]_m$ were synchronized to the rising phase of the $[Ca^{2+}]_c$ signal in the discrete regions of Ca^{2+} release, whereas no $[Ca^{2+}]_m$ increase was observed at other locations (Fig. 1*A*, images ix–xiii, and *B*). By contrast, a global $[Ca^{2+}]_m$ increase was coupled to the diffuse Ca^{2+} release mediated by maximally activated RyR (Fig. 1*A*, image xiv, and *B*). $[Ca^{2+}]_m$ increases never preceded the $[Ca^{2+}]_c$ rise and showed slower decay than the $[Ca^{2+}]_c$ transients (Fig. 1*B*). Furthermore, the $[Ca^{2+}]_c$ and $[Ca^{2+}]_m$ responses displayed region-specific amplitude and temporal patterns during $[Ca^{2+}]_c$ spiking restricted to subdomains of the cells (Fig. 1). Localized coupling of $[Ca^{2+}]_c$ and $[Ca^{2+}]_m$ spikes were also observed when addition of ryanodine or Ca^{2+} was used to activate the RyR (not shown). The amplitude of the locally restricted $[Ca^{2+}]_c$ and $[Ca^{2+}]_m$ spikes typically were smaller than those during global responses (Fig. 1*B*). The magnitude of the F_{rhod2} rise from $[Ca^{2+}]_m$ signals confined to <10-μm-diameter regions was 21.7 ± 2.3% of the F_{rhod2} increase obtained during global $[Ca^{2+}]_c$ signals ($n = 16$). These results suggest that in permeabilized myotubes, suboptimal stimulation of RyR triggers localized $[Ca^{2+}]_c$ spikes that are coupled to localized, submaximal $[Ca^{2+}]_m$ transients.

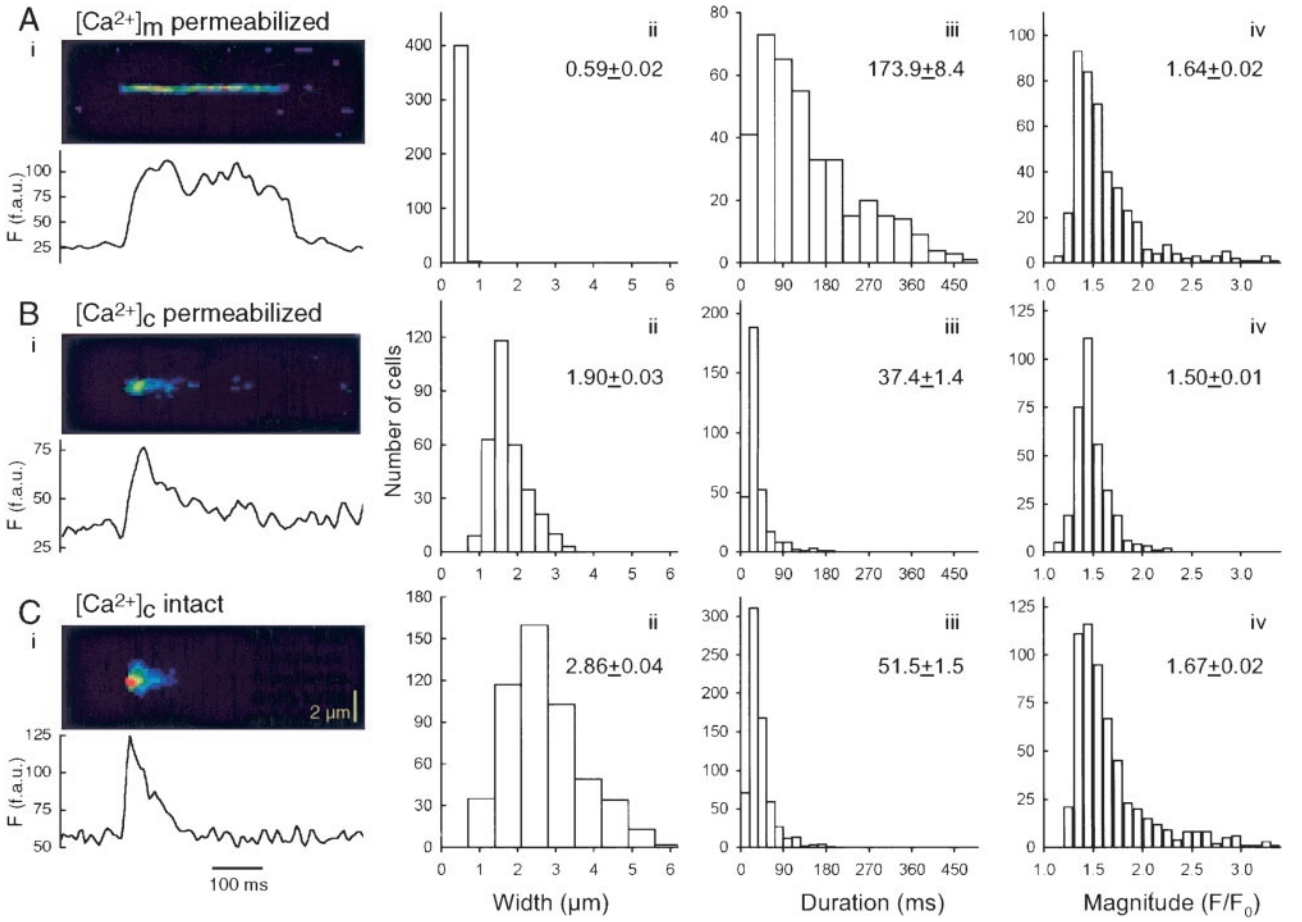

Fig. 4. Elementary events of the RyR-mediated $[Ca^{2+}]_c$ and $[Ca^{2+}]_m$ signal. Confocal line scanning was carried out in intact (*C*) or in permeabilized (*A* and *B*) myotubes by using fluo3 to monitor $[Ca^{2+}]_c$ (*B* and *C*) or rhod2 to monitor $[Ca^{2+}]_m$ (*A*). In all cases, the myotubes were exposed to 0.25 mM caffeine. The linescan images are oriented so that time is on the horizontal axis. Width, duration, and magnitude histograms for the local $[Ca^{2+}]$ transients are also shown ($n = 350–550$).

Based on the area of activation, the localized $[Ca^{2+}]_m$ signals shown in Fig. 1 could be derived from small groups of mitochondria. To discriminate the contributions of individual mitochondria, we used confocal imaging of $[Ca^{2+}]_c$ and $[Ca^{2+}]_m$ with fluo3 added to the permeabilized cells and compartmentalized rhod2, respectively. First, we recorded two-dimensional images during sequential stimulation of the cells with submaximal and maximal doses of caffeine. When 1 and 10 mM caffeine was added, both doses yielded transient $[Ca^{2+}]_c$ increases that appeared as global $[Ca^{2+}]_c$ responses, and each was coupled to a $[Ca^{2+}]_m$ elevation that manifested in discrete structures (Fig. 2*A Top*). The spatial distribution of the $[Ca^{2+}]_c$ and $[Ca^{2+}]_m$ responses was visualized by using a three-dimensional presentation (Fig. 2*A Middle* and *Bottom*). This presentation underscores that $[Ca^{2+}]_c$ elevations took place throughout the cytoplasm during each response (Fig. 2*A*, xi and xiii; the nucleus exhibited above-average fluo3 labeling), whereas the $[Ca^{2+}]_m$ increases were manifest as discrete peaks corresponding to individual mitochondria or clusters of a few mitochondria (Fig. 2*A*, vii and ix). Based on electron microscopic evaluation of the ultrastructure of myotubes, many of the mitochondria are oval-shaped (diameter of <1 μm), whereas some mitochondria appear as long tubular structures (21). As shown by comparison of peak heights between images vii and ix, the $[Ca^{2+}]_m$ response was maximal during the first step of stimulation for some mitochondria, whereas other mitochondria exhibited a considerably larger response to maximal caffeine. Because mitochondrial Ca^{2+} uptake sites do not appear to exhibit intrinsic heterogeneity (13, 24), subcellular heterogeneity in the mitochondrial sensitivity to RyR-mediated $[Ca^{2+}]_c$ signal may reflect differences in Ca^{2+} release flux in the immediate vicinity of the mitochondria.

A more striking attenuation of the $[Ca^{2+}]_m$ signal exhibited by the mitochondria occurred when a localized RyR-mediated $[Ca^{2+}]_c$ elevation was elicited with caffeine (0.5 mM; as in Fig. 1). The only mitochondria displaying a $[Ca^{2+}]_m$ rise were at the center of $[Ca^{2+}]_c$ signals (Fig. 2*B*, ii; three-dimensional presentation in x), whereas the other mitochondria in the vicinity remained silent (ii vs. iv). Time courses for the region of the responsive mitochondrion revealed a $[Ca^{2+}]_c$ spike lasting a few seconds and a relatively small and more slowly decaying $[Ca^{2+}]_m$ increase (Fig. 2*B*, ix). Taken together, the two-dimensional confocal imaging studies revealed the fundamental structures exhibiting the $[Ca^{2+}]_m$ rise during RyR-mediated Ca^{2+} release. These studies demonstrated that the number of responding mitochondria, as well as the amplitude of single mitochondrial $[Ca^{2+}]$ increases, increase with the extent of RyR activation. Thus, the question arises of whether activation of a few release sites during a single $[Ca^{2+}]_c$ spark with the typical small amplitude and 100- to 200-ms decay (2), is sufficient to increase the activity of mitochondrial Ca^{2+} uptake and sufficient to elevate $[Ca^{2+}]_m$ in a mitochondrion.

Because of the temporal limitations of two-dimensional confocal imaging, we used high-speed scanning along a single line to visualize the elementary events of the cytosolic and mitochondrial calcium signal. First, we carried out linescan imaging of $[Ca^{2+}]_c$ in fluo3-loaded intact myotubes. In cells exposed to a low dose of caffeine (0.25 mM), which failed to cause propagating $[Ca^{2+}]$ response,

spatially localized and short-lived $[Ca^{2+}]_c$ signals were recorded (Fig. 3*A*). As described in other systems (25, 26), similar events were seen at a lower frequency in the absence of caffeine. These $[Ca^{2+}]_c$ events were smaller and much shorter than the events shown in Figs. 1 and 2 and displayed properties very similar to Ca^{2+} sparks in other systems [width at half-maximal amplitude, 2.86 ± 0.04 μm, amplitude (F/F_0) 1.67 ± 0.02 and duration at half-maximal amplitude, 51.5 ± 1.5 ms; Fig. 4*C*]. Consistent with recent observations (27–29), we could also record miniature Ca^{2+} release events in permeabilized myotubes with fluo3 added to the cytosolic buffer (Fig. 4*B*). Based on their spatiotemporal pattern, these events represent RyR-mediated $[Ca^{2+}]_c$ sparks in the H9c2 cardiac myotubes. Therefore, we used the conditions in which $[Ca^{2+}]_c$ sparks were generated in this preparation to investigate whether elementary Ca^{2+} release events are delivered to the mitochondria.

Confocal linescan imaging revealed the presence of highly localized (<1 μm), subsecond F_{rhod2} transients in the permeabilized myotube model (Fig. 3*B*). These fluorescence responses were dependent on Ca^{2+} release from sarcoplasmic reticulum and also on mitochondrial Ca^{2+} uptake, because predepletion of the sarcoplasmic reticulum store with a Ca^{2+} pump inhibitor, thapsigargin (2 μM, $n = 5$, not shown), or elimination of the driving force of mitochondrial Ca^{2+} uptake by uncoupler (FCCP; 5 μM, $n = 5$, not shown) prevented the F_{rhod2} transients. In contrast to Ca^{2+} sparks, the F_{rhod2} transients did not show lateral spreading, which can be explained by the mitochondrial membrane acting as a Ca^{2+} diffusion barrier (Fig. 3*B*). Properties of the highly localized F_{rhod2} transients recorded in myotubes are summarized in Fig. 4*A*. The diameter of these events was 0.59 ± 0.02 μm at half-width (Fig. 4*A*, ii), suggesting that the $[Ca^{2+}]$ rise took place in individual mitochondria. The magnitude of the single mitochondrial $[Ca^{2+}]_m$ increases was estimated to be 200–400 nM (see *Experimental Procedures*). The mean duration was 174 ± 8.4 ms at half-height (Fig. 4*A*, iii), illustrating the relatively slow decay of the miniature $[Ca^{2+}]_m$ elevations. However, we also observed events that showed rapid decline similar to the sparks (Fig. 3*B*, v; broad distribution of duration is shown in Fig. 4*A*, iii). Collectively, these data suggest that $[Ca^{2+}]_m$ increases restricted to single mitochondria are coupled to elementary Ca^{2+} release events in myotubes. Because the miniature $[Ca^{2+}]_m$ increases represent the mark left by $[Ca^{2+}]_c$ sparks on $[Ca^{2+}]_m$, we refer to these fundamental mitochondrial events as "Ca^{2+} marks." The spatiotemporal differences between the elementary cytosolic and mitochondrial signals are underscored by three-dimensional plots of the individual events (Fig. 3*C*). Specifically, $[Ca^{2+}]_c$ sparks were relatively broad in the spatial domain, but dissipate rapidly in time, reflecting diffusion of released Ca^{2+} from the spark site (Fig. 3*C Upper*). By contrast, $[Ca^{2+}]_m$ marks occupy a small area with sharp edges, because of restriction of diffusion of Ca^{2+} by the mitochondrial membrane (Fig. 3*C Lower*). $[Ca^{2+}]_m$ marks were also more prolonged than $[Ca^{2+}]_c$ sparks. Interestingly, $[Ca^{2+}]_m$ marks are confined to a considerably smaller area than the localized mitochondrial depolarizations reported by Duchen *et al.* (19) in myocytes. Because mitochondria have been proposed to form a functional syncytium (7) and an electrically coupled network (30), depolarization could propagate from one mitochondrion to the next. However, based on photobleaching experiments, Park *et al.* (13) have proposed that mitochondria are not necessarily luminally connected, and our data suggest that small $[Ca^{2+}]_m$ elevations do not display luminal spreading.

To better understand how Ca^{2+} sparks leave their marks on $[Ca^{2+}]_m$, we evaluated the spatial distribution of Ca^{2+} marks. In the majority of linescan frames examined (397 of 509, 3,072 ms each), the $[Ca^{2+}]_m$ signal appeared to derive from only one mitochondrion (<1 μm in half-width). In the other linescan images in which Ca^{2+} marks were characterized, either the spatial separation of marks was >2.5 μm (110 of 509) or more closely apposed mitochondria were activated with >100-ms temporal separation (2 of 509). In light of these data, we conclude that a spark is not likely to result in more than one Ca^{2+} mark. To determine the fraction of sparks that propagates to the mitochondria, we calculated the number of regions in permeabilized myotubes that displayed $[Ca^{2+}]_c$ sparks and $[Ca^{2+}]_m$ marks, respectively. The frequency of $[Ca^{2+}]_c$ sparks was 60% higher than the frequency of $[Ca^{2+}]_m$ marks (0.36 ± 0.05/frame, 15 experiments; 0.22 ± 0.08/frame, 13 experiments). We also attempted to record $[Ca^{2+}]_m$ marks simultaneously with $[Ca^{2+}]_c$ sparks. However, these experiments were not successful because of the relatively low fluorescence signal associated with marks and reduced signal-to-noise ratio in our multiparameter measurements. Other factors also may limit the occurrence of Ca^{2+} marks. Not all mitochondria are immediately adjacent to the sarcoplasmic reticulum surface (e.g., refs. 7 and 21) and mitochondrial Ca^{2+} uptake sites exhibit low affinity to Ca^{2+}, suggesting that $[Ca^{2+}]_c$ sparks may occur unrecognized by mitochondria (as reported for $[Ca^{2+}]_c$ puffs in HeLa cells; ref. 31). Because mitochondrial Ca^{2+} uptake sites display Ca^{2+}-induced sensitization (32), during repetitive sparks, the first event may sensitize uptake sites such that only subsequent sparks are delivered into the mitochondrion. Despite the above-mentioned limitations of $[Ca^{2+}]_c$ spark propagation to mitochondria, after the addition of mitochondrial inhibitors, we observed a 2-fold increase in the frequency of sparks (see below). This result also suggests activation of mitochondrial Ca^{2+} uptake by a substantial fraction of $[Ca^{2+}]_c$ sparks and implies that mitochondria may directly accumulate Ca^{2+} from activated clusters of RyR, preventing the generation of $[Ca^{2+}]_c$ sparks.

The variations in decline, the relatively long mean half-time, and restricted lateral spreading of $[Ca^{2+}]_m$ marks suggest that mechanisms other than diffusion are involved in the falling phase. Recently, we have shown that deactivation of $[Ca^{2+}]_m$ spikes during global $[Ca^{2+}]_c$ oscillations use the mitochondrial Ca^{2+} exchanger, whereas no major contribution of the permeability transition pore was found (22). Thus, we studied the effect of CGP37157, an inhibitor of the Ca^{2+} exchanger, on the duration of $[Ca^{2+}]_m$ marks to determine whether carrier-mediated mitochondrial Ca^{2+} efflux

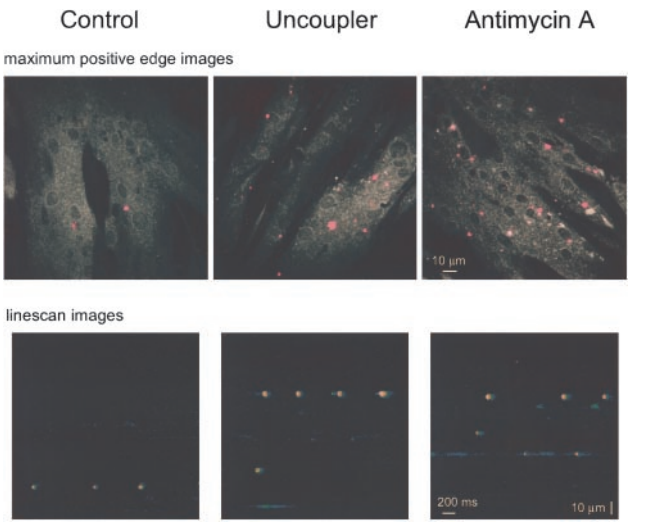

Fig. 5. Mitochondrial Ca^{2+} uptake controls $[Ca^{2+}]_c$ sparks in intact myotubes. (*Upper*) Two-dimensional images of localized $[Ca^{2+}]_c$ signals recorded in fluo3-loaded myotubes exposed to solvent (*Left*), FCCP (5 μM, Uncoupler; *Center*), or antimycin A (5 μM, *Right*) in the presence of oligomycin. The gray images show the fluo3 fluorescence. The purple overlays show the maximal fluorescence increase for each pixel (maximal positive edge), calculated by subtraction of sequential images in 15 image sequences. Thus, the overlays indicate all regions that displayed $[Ca^{2+}]_c$ responses during the image series. (*Lower*) Linescan images showing $[Ca^{2+}]_c$ sparks in fluo3-loaded myotubes exposed to solvent (*Left*), FCCP (5 μM, Uncoupler; *Center*), or antimycin A (5 μM, *Right*) in the presence of oligomycin.

is important in recovery of the elementary events. In cells displaying $[Ca^{2+}]_m$ marks, CGP37157 (10 μM) resulted in prolongation of the elementary events (215.9 ± 19.5 and 374.3 ± 40.9 ms at half-height, before and after addition of CGP37157, $n = 64$ and 63, $P < 0.001$). By contrast, CGP37157 failed to change the duration of $[Ca^{2+}]_c$ sparks (47.9 ± 0.8 vs. 44.0 ± 0.6 ms in the presence and absence of CGP37157, $n = 616$ and 814). Taken together, these data suggest that decay of $[Ca^{2+}]_m$ marks is dependent on carrier-mediated Ca^{2+} extrusion from the mitochondria. Although the Ca^{2+} exchanger has been demonstrated to control the decay of $[Ca^{2+}]_m$ increases in many cell types, our result shows that in contrast to cytosolic and nucleoplasmic elementary Ca^{2+} signals, $[Ca^{2+}]_m$ marks do not simply decay by diffusion. In addition to the role of the Ca^{2+} exchanger demonstrated in this study, CGP37157-insensitive efflux pathways as well as slow intramitochondrial Ca^{2+} buffering may also contribute to the decay of marks. Regulation of the life-time of $[Ca^{2+}]_m$ marks by mitochondrial transporters yields another difference between $[Ca^{2+}]_c$ sparks and $[Ca^{2+}]_m$ marks and allows these efflux pathways to modulate the mitochondrial targets of the $[Ca^{2+}]_m$ mark as well as to exert feedback on $[Ca^{2+}]_c$.

Several mitochondrial dehydrogenases are sensitive to $[Ca^{2+}]_m$ changes in the submicromolar range (14), and imaging studies on the coupling between gradual increases in $[Ca^{2+}]_m$ and NAD(P)H fluorescence have suggested that relatively small increases in $[Ca^{2+}]_m$ may be sufficient to stimulate mitochondrial metabolism (8). However, with current imaging technology, we could not resolve an NAD(P)H increase resulting from propagation of a single $[Ca^{2+}]_c$ spark to an individual mitochondrion. Recent studies also have demonstrated multiple feedback effects of mitochondrial Ca^{2+} uptake on $[Ca^{2+}]_c$ signaling during the course of global calcium signals (for review, see refs. 33–37) and that mitochondria may sequester 25–50% of mobilized Ca^{2+} (21). To evaluate the physiological significance of the mitochondrial Ca^{2+} uptake during $[Ca^{2+}]_m$ marks in elementary $[Ca^{2+}]_c$ signaling, we studied the effect of mitochondrial Ca^{2+} uptake blockers on spontaneous $[Ca^{2+}]_c$ sparks in intact myotubes. Treatment with uncoupler (5 μM FCCP) or antimycin A (5 μM), in the presence of oligomycin to prevent cellular ATP depletion, resulted in a considerable increase in the number and size of localized $[Ca^{2+}]_c$ increases recorded in two-dimensional images (Fig. 5 *Upper*). Furthermore, the $[Ca^{2+}]_c$ sparks displayed increased frequency, duration, and width in linescan images (Fig. 5 *Lower*). On average, mitochondrial inhibitors caused a 2-fold increase in the frequency of $[Ca^{2+}]_c$ sparks (control, 3.2 ± 0.3; FCCP + oligomycin, 6.5 ± 0.6; and antimycin + oligomycin, 7.7 ± 0.8 $mm^{-1} \times s^{-1}$; $n = 814$, 477, and 299). The mean duration and spatial size of the $[Ca^{2+}]_c$ sparks was also increased by 20–30% in FCCP or antimycin-pretreated cells [FCCP + oligomycin, 119%, and antimycin + oligomycin, 130% of control (duration at half-height); FCCP + oligomycin, 124% and antimycin + oligomycin, 125% of control (half-width)]. These changes could arise, in part, from an increase in global $[Ca^{2+}]_c$. However, FCCP caused only a small rise in $[Ca^{2+}]_c$ under these conditions (data not shown). Thus, the data demonstrate that delivery of $[Ca^{2+}]_c$ sparks to the mitochondria also may result in an important feedback regulation of the elementary $[Ca^{2+}]_c$ signals. As a consequence, mitochondria could serve to suppress the excitability of the excitation–contraction coupling system by reducing spark frequency and size.

Our data reveal that $[Ca^{2+}]_c$ sparks permit delivery of Ca^{2+} to neighboring mitochondria, giving rise to $[Ca^{2+}]_m$ marks. Thus, elementary $[Ca^{2+}]_c$ signaling may allow for asynchronous regulation of functionally discrete mitochondria. Calcium marks are confined to individual mitochondria and are likely to have smaller amplitude than the $[Ca^{2+}]_m$ elevations occurring when numerous elementary events are summated to give rise to a regenerative $[Ca^{2+}]_c$ wave. This may be because the open time of a given cluster of RyR is longer during a regenerative $[Ca^{2+}]_c$ wave than that during a $[Ca^{2+}]_c$ spark, or each mitochondrion may sense $[Ca^{2+}]_c$ sparks originated from more than one cluster of RyR. Nevertheless, elementary mitochondrial Ca^{2+} uptake events appear to contribute to the organization of elementary calcium signaling in the cytosol and may also establish control over the mitochondrial Ca^{2+} targets. Importantly, we also demonstrated that $[Ca^{2+}]_m$ marks dissipate relatively slowly and use exchanger-mediated Ca^{2+} export in their decay phase. The prolongation of marks compared with cytosolic sparks may facilitate activation of the Ca^{2+}-sensitive targets in the mitochondrial matrix and also may support localized recharging of the sarcoplasmic reticulum Ca^{2+} store after the RyR cease to fire. Thus, we propose that the elementary events of calcium signaling involve mitochondrial contributions, which establish precise, localized control of $[Ca^{2+}]_m$-dependent mitochondrial functions.

We thank Drs. T. Pozzan, S. Györke, S. K. Joseph, and J. B. Hoek for valuable discussions and Paul Anderson for his help with software development. This work was supported by grants from the American Heart Association and National Institutes of Health (to G.H.). G.H. is a recipient of a Burroughs Wellcome Fund Career Award. P.P. is a recipient of a Juvenile Diabetes Foundation Postdoctoral Fellowship.

1. Parker, I. & Yao, Y. (1991) *Proc. R. Soc. London Ser. B* **246,** 269–274.
2. Cheng, H., Lederer, W. J. & Cannell, M. B. (1993) *Science* **262,** 740–744.
3. Bootman, M. D., Berridge, M. J. & Lipp, P. (1997) *Cell* **91,** 367–373.
4. Berridge, M. J., Bootman, M. D & Lipp, P. (1998) *Nature (London)* **395,** 645–648.
5. Jaggar, J. H., Porter, V. A., Lederer, W. J. & Nelson, M. T. (2000) *Am. J. Physiol. Cell Physiol.* **278,** C235–C256.
6. Rizzuto, R., Brini, M., Murgia, M. & Pozzan, T. (1993) *Science* **262,** 744–747.
7. Rizzuto, R., Pinton, P., Carrington, W., Fay, F. S., Fogarty, K. E., Lifshitz, L. M., Tuft, R. A. & Pozzan, T. (1998) *Science* **280,** 1763–1766.
8. Hajnóczky, G., Robb-Gaspers, L. D., Seitz, M. B. & Thomas, A. P. (1995) *Cell* **82,** 415–424.
9. Lawrie, A. M., Rizzuto, R., Pozzan, T. & Simpson, A. W. (1996) *J. Biol. Chem.* **271,** 10753–10759.
10. Simpson, P. B. & Russell, J. T. (1996) *J. Biol. Chem.* **271,** 33493–33501.
11. Csordás, G., Thomas, A. P. & Hajnóczky, G. (1999) *EMBO J.* **18,** 96–108.
12. Monteith, G. R. & Blaustein, M. P. (1999) *Am. J. Physiol.* **276,** C1193–C1204.
13. Park, M. K., Ashby, M. C., Erdemli, G., Petersen, O. H. & Tepikin, A. V. (2001) *EMBO J.* **20,** 1863–1874.
14. McCormack, J. G., Halestrap, A. P. & Denton, R. M. (1990) *Physiol. Rev.* **70,** 391–425.
15. Duchen, M. R. (1992) *Biochem. J.* **283,** 41–50.
16. Jouaville, L. S., Pinton, P., Bastianutto, C., Rutter, G. A. & Rizzuto, R. (1999) *Proc. Natl. Acad. Sci. USA* **96,** 13807–13812.
17. Szalai, G., Krishnamurthy, R. & Hajnóczky, G. (1999) *EMBO J.* **18,** 6349–6361.
18. Chacon, E., Ohata, H., Harper, I. S., Trollinger, D. R., Herman, B. & Lemasters, J. J. (1996) *FEBS Lett.* **382,** 31–36.
19. Duchen, M. R., Leyssens, A. & Crompton, M. (1998) *J. Cell Biol.* **142,** 975–988.
20. Robb-Gaspers, L. D., Burnett, P., Rutter, G. A., Denton, R. M., Rizzuto, R. & Thomas, A. P. (1998) *EMBO J.* **17,** 4987–5000.
21. Pacher, P., Csordás, G., Schneider, T. & Hajnóczky, G. (2000) *J. Physiol.* **529,** 553–564.
22. Szalai, G., Csordás, G., Hantash, B. M., Thomas, A. P. & Hajnóczky, G. (2000) *J. Biol. Chem.* **275,** 15305–15313.
23. Collier, M. L., Thomas, A. P. & Berlin, J. R. (1999) *J. Physiol.* **516,** 117–128.
24. Pozzan, T. & Rizzuto, R. (2000) *Nat. Cell Biol.* **2,** 25–27.
25. Satoh, H., Katoh, H., Velez, P., Fill, M. & Bers, D. M. (1998) *Circ. Res.* **83,** 1192–1204.
26. Conklin, M. W., Powers, P., Gregg, R. G. & Coronado, R. (1999) *Biophys. J.* **76,** 657–669.
27. Lukyanenko, V. & Gyorke, S. (1999) *J. Physiol.* **521,** 575–585.
28. Gonzalez, A., Kirsch, W. G., Shirokova, N., Pizarro, G., Brum, G., Pessah, I. N., Stern, M. D., Cheng, H. & Rios, E. (2000) *Proc. Natl. Acad. Sci. USA* **97,** 4380–4385.
29. Shtifman, A., Ward, C. W., Wang, J., Valdivia, H. H. & Schneider, M. F. (2000) *Biophys. J.* **79,** 814–827.
30. De Giorgi, F., Lartigue, L. & Ichas, F. (2000) *Cell Calcium* **28,** 365–370.
31. Collins, T. J., Lipp, P., Berridge, M. J. & Bootman, M. D. (2001) *J. Biol. Chem.* **276,** 26411–26420.
32. Kröner, H. (1986) *Arch. Biochem. Biophys.* **251,** 525–535.
33. Babcock, D. F. & Hille, B. (1998) *Curr. Opin. Neurobiol.* **8,** 398–404.
34. Duchen, M. R. (1999) *J. Physiol.* **516,** 1–17.
35. Hajnóczky, G., Csordás, G., Madesh, M. & Pacher, P. (2000) *J. Physiol.* **529,** 69–81.
36. Rizzuto, R., Bernardi, P. & Pozzan, T. (2000) *J. Physiol.* **529,** 37–47.
37. Rutter, G. A. & Rizzuto, R. (2000) *Trends Biochem. Sci.* **25,** 215–221.